Characteristics of Torque around Axial Direction on Cylindrical Rotating Detonation Engines

Satoru Sawada[1)], Kazuki Ishihara[1)], Noboru Itouyama[2)], Hiroaki Watanabe[3)], Akira Kawasaki[4)], Ken Matsuoka[1)], Jiro Kasahara[2)], Akiko Matsuo[5)], and Ikkoh Funaki[6)]

[1)] Department of Aerospace Engineering, Nagoya University, Nagoya, Japan
[2)]Institute of Materials and Systems for Sustainability, Nagoya University, Nagoya, Japan
[3)]Department Fluides, Thermique et Combustion, ENSMA, Chasseneuil du Poitou, France
[4)]Department of Mechanical Engineering, Shizuoka University, Hamamatsu, Japan
[5)]Department of Mechanical Engineering, Keio University, Yokohama, Japan
[6)]Japan Aerospace Exploration Agency (JAXA), Sagamihara, Kanagawa, Japan

1 Introduction

In the case of detonation combustion, a supersonic combustion wave propagates in a premixed fuel and oxidizer mixture. Since the velocity of propagation is on the order of kilometers per seconds, the reaction zone is relatively small. Because the advantage shortens time to complete combustion, the size of the combustor achieves more compact size than the conventional one [1].

There are several types of detonation engines which obtain energy from detonation combustion [1]. Rotating detonation engines (RDEs) utilize one or more supersonic combustion waves that continuously propagate inside annular or cylindrical combustion chamber [2]. Due to the simple and compact geometry of combustor, RDEs have attracted attention as one of next-generation technologies for space transportation system and power plant system.

One of the characteristics of RDEs is a swirl inside the combustion chamber. Fig. 1 explains the mechanism. Since rotating detonation waves accelerate gas in the azimuthal direction, gas behind rotating detonation waves contains huge amount of the azimuthal component of velocity, v_θ. v_θ is related to the thrust performance because v_θ consumes a part of the kinetic energy on the exit plain of the RDEs combustion chamber. In addition, v_θ generates torque around the axial direction of RDEs, T_z, due to the gradient of v_θ in the radial direction, r, around the wall and the azimuthal component of the shear stress, τ_θ, on the combustion chamber wall. In a previous study, the effect of performance was evaluated via the measurement of the torque generated around the axial direction of RDEs [3]. The swirl, however, has applications such as a gas turbine system. Braun et al. demonstrated an annular RDEs with the wavy surface on the side wall via a numerical calculation [4]. He revealed characteristics of the torque induced by pressure difference derived from the swirl on the wavy surface. On the other hand, the system requires long duration of operation. Cylindrical RDEs, however, has an advantage for the thermal issue because cylindrical RDEs are composed of less components which potentially have the thermal damage by removing the inner column. A problem is the decrease of the wetted perimeter length, l_H, between the rotating detonation waves and the combustion chamber wall. In this manuscript, the effect was evaluated by comparing T_z of annular RDEs and cylindrical RDEs in experiment. The potential to generate v_θ around the combustion chamber wall was proven.

Correspondence to: sawada.satoru.e0@s.mail.nagoya-u.ac.jp

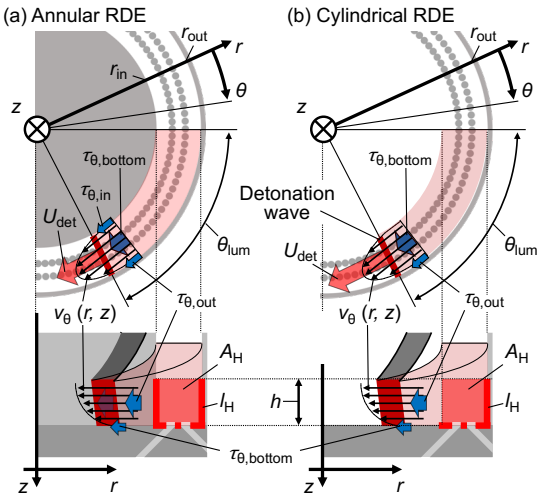

Figure 1: Schematics of the azimuthal component of velocity and shear stress on the wall of (a) an annular RDE and (b) a cylindrical RDE.

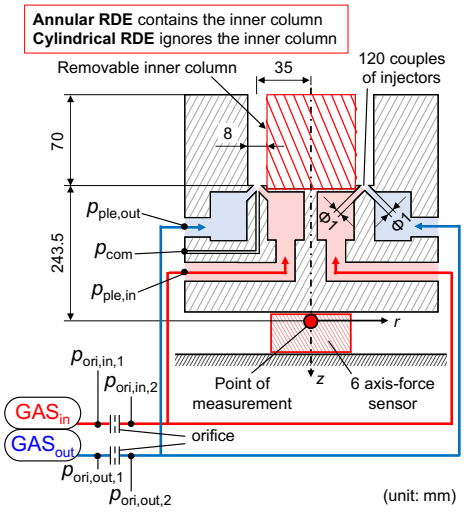

Figure 2: A geometry of an RDE, a frame of reference, distribution of measurement points of sensors, and a propellant supply system.

2 Experiment Setup

Figure 2 is a geometry of an experimental. The RDE was made of copper and composed of plenum rooms for propellants, 120 pairs of doublet injectors, 39 mm radius outer wall and 31 mm radius inner wall. Each injector was 1 mm diameter, and the axial length of inner and outer walls were 70 mm. We controlled the propellants supply condition via orifices in Fig. 2. The mass flow rate and the equivalence ratio were calculated with pressure data from piezoelectric pressure sensors at upstream and downstream of the orifices. The propellants were supplied into the plenum room without the azimuthal component of velocity. We supplied gaseous oxygen and gaseous ethylene from the injectors. The propellant impinged on the 35 mm radius circle. We defined the radius as the mean radius, r_m. In addition, the inner column of the RDE was removable. When the RDE has the inner column, the combustion chamber became annular cross section (an annular RDE). When the inner column was removed, the combustion chamber had cylindrical cross section (a cylindrical RDE). A case of supplying ethylene from the inner injectors and oxygen from the outer injectors in the annular RDE, and in the cylindrical RDE were defined as "A-iF-oO" and "C-iF-oO" respectively. A case of supplying oxygen from the inner injectors and ethylene from the outer injectors in the cylindrical RDE was defined as "C-iO-oF."

T_z was measured with the 6-axis force sensor which was capable of measuring force in the 3 axes and torque around each axis simultaneously. The RDE was set on the 6-axis force sensor with the combustion chamber exit facing up to prevent the damage of sensor from the burned gas. Fig. 2 indicates the frame of reference. The r axis was defined as from the center of the RDE toward the radial direction. The z axis was the axial direction of the RDE, and the positive direction was from the combustion chamber exit to the bottom. The θ axis was the azimuthal direction around the z axis. The measurement point of the 6-axis force sensor was on the z axis of the RDE.

Figure 3 explains the measurement system inside a vacuum chamber. The inside of combustion chamber was observed in the axial direction via three mirrors. The optical path reflected three times and reached the window on the side wall of the vacuum chamber. The detonation waves inside the RDE were observed with a high-speed camera (Phantom 2011; Vision Research, Birmingham, Alabama) outside of the vacuum chamber. The sampling frequency and the resolution were 180258 Hz and 256 × 256, and 430769 Hz and 128 × 128.

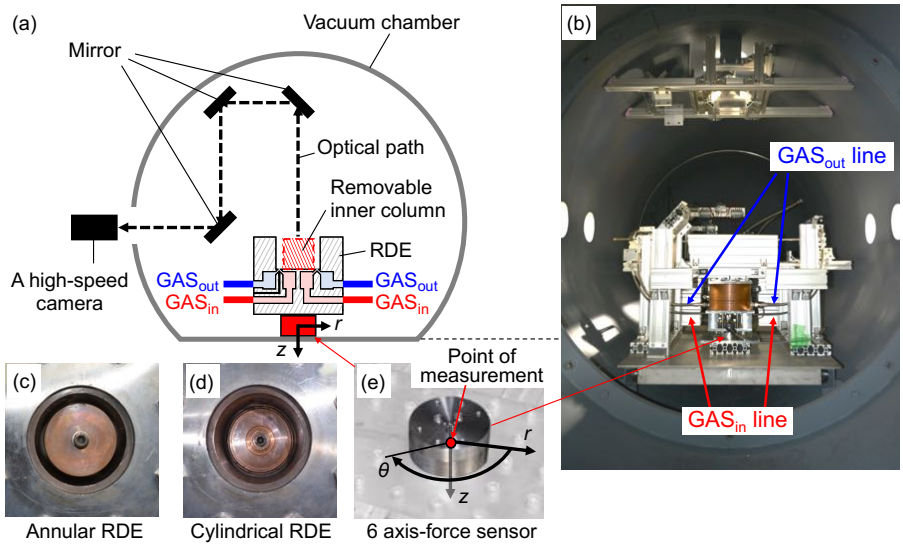

Figure. 3: (a) a schematic of distribution inside the vacuum chamber, views of (b) inside the vacuum chamber, (c) the annular RDE, (d) the cylindrical RDE, and (e) the 6-axis force sensor.

3 Results and Discussion

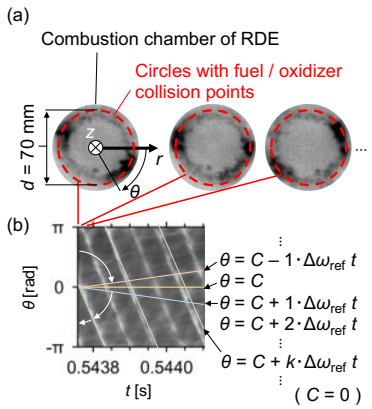

Figure 4: Examples of (a) the θ - t diagram, (b) the velocity of frame of reference vs the frequency vs the power spectral.

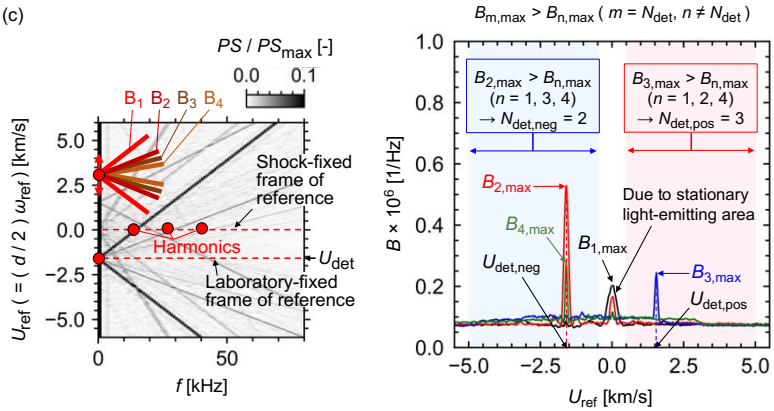

Figure 5: Definitions of the detonation velocity and the number of detonation waves.

In this study, the propagation velocity of detonation waves was defined as the velocity of light-emitting zone. In order to decide the propagation mode of detonation waves Circuit Wave Analysis (CWA) [5] was applied. Fig. 4 (a) is an example of a diagram with the azimuthal axis and the time axis (θ - t diagrams). In the diagrams, sampling luminosity values of the same location in a frame of reference rotating at an angular speed, ω_{ref}, means sampling the value along the oblique line $\theta = C + \omega_{ref} t$. Fig. 4 (c) is the result of Fast Fourier Transform (FFT) of luminosity values in each case of ω_{ref}. In the figure, $\omega_{ref} = 0$ means the result of FFT in a shock-fixed frame of reference. As the difference between rotating velocity of frame of reference, U_{ref} ($= r_m \omega_{ref}$), approaches to the velocity of detonation wave, U_{det}, the peaks of Power Spectral (PS) shifts to zero, and vice versa. It results in "V" shape line which intersect with the axis of U_{ref} at U_{det}. In this study, $C = 0$, ΔU_{ref} ($= r_m \Delta\omega_{ref}$) = 25 m/s, and CWA was applied per 256 frames for the frame rate of 180258 fps, and per 512 frames for the frame rate of 430769 fps.

The angle of "V" shape line depends on the resolution of FFT, $\Delta\omega_{ref}$, and the number of light-emitting area, N_{det}. Chacon, F., and Gamba, M. suggested comparing the combination of U_{ref} which intersects with an arbitrary "V" shape line and the sum of PS on the "V" shape line with the angle for each N_{det}, B. Fig. 5 is an example of comparison of B and U_{ref}. Note that the subscript of B is an arbitrary value of N_{det} corresponding to the angle of an arbitrary "V" shape line, N_{arb}. When the B_{Narb} is the maximum, $N_{det} = N_{arb}$ in one direction and within the limited range of U_{ref}. In this study, the ranges of positive and negative U_{ref} were defined as -5 km/s to 0 km/s (the suffix "neg") and 0 km/s to 5 km/s (the suffix "pos"), respectively. U_{det} and N_{det} were defined as U_{ref} and N_{arb} when B_{Narb} is the maximum within each range. CWA was demonstrated in the case of N_{arb} = 1 to 4.

Figure 6 (a-c) is schematics of the geometry and the injectors conditions. As Fig. 6 (d, e) indicates, mass flow rate, $\dot{m}$, equivalence ratio, ER, and back pressure, P_b, were controlled within 0.013-0.106 kg/s, 0.97-1.53 [-], and 11.8-101.5 [kPa]. Fig. 7 indicates the time mean value of T_z and deviation of $B_{sum,max}$ of positive and negative direction ($B_{sum} = \sum B_{Narb}$). As B depends on the luminosity values, the balance

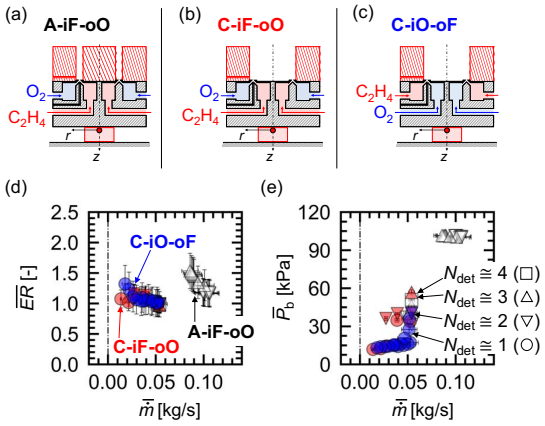

Figure 6: Schematics of (a) A-iF-oO, (b) C-iF-oO, (c) C-iO-oF, (d) the equivalence ratio vs the mass flow rate, and (e) the back pressure vs the mass flow rate.

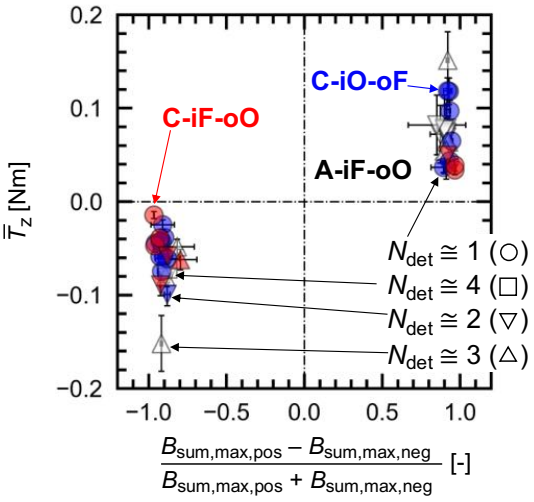

Figure 7: The torque vs the deviation of light emission intensity between positive and negative propagation.

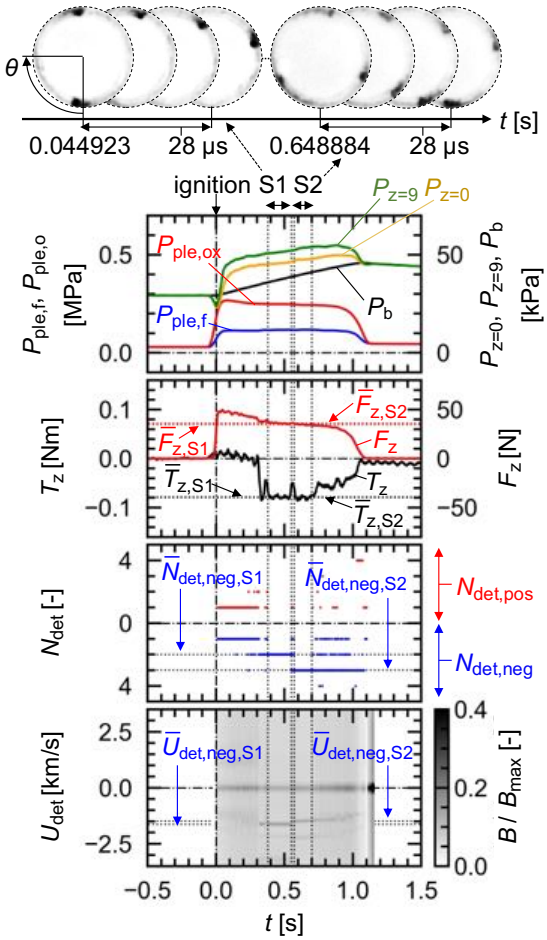

Figure 8: (a) Example images of rotating detonation waves, and the time record of (b) the pressure, the thrust, the torque, the number of detonation waves result of CWA (from the top) in the test of A-iF-oO under mass flow rate 0.048-0.054 kg/s.

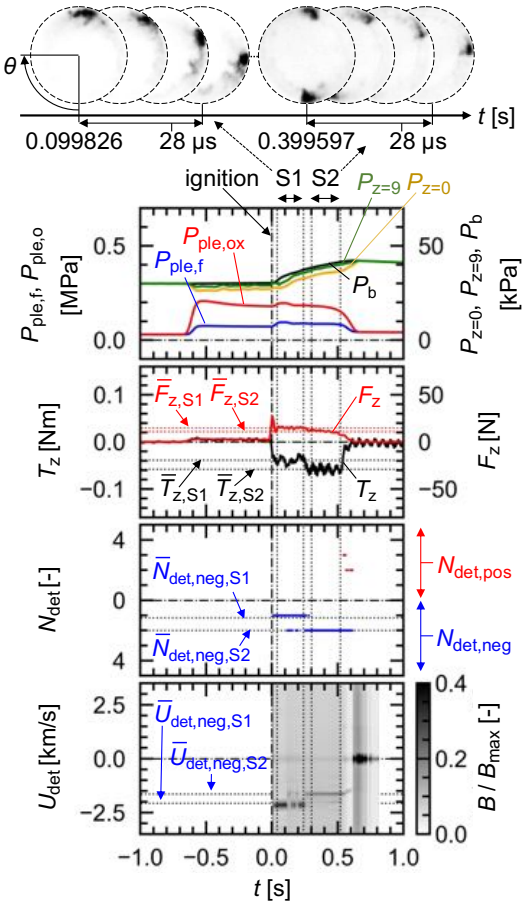

Figure 9: (a) Example images of rotating detonation waves, and the time record of (b) the pressure, the thrust, the torque, the number of detonation waves result of CWA (from the top) in the test of C-iF-oO under mass flow rate 0.039 kg/s.

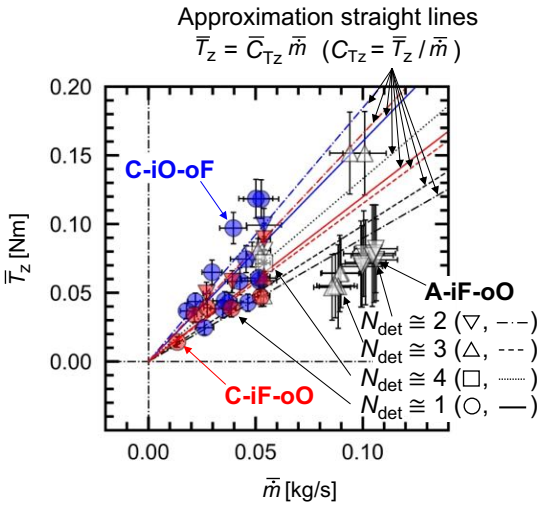

Figure 10: The torque vs the mass flow rate detonation waves.

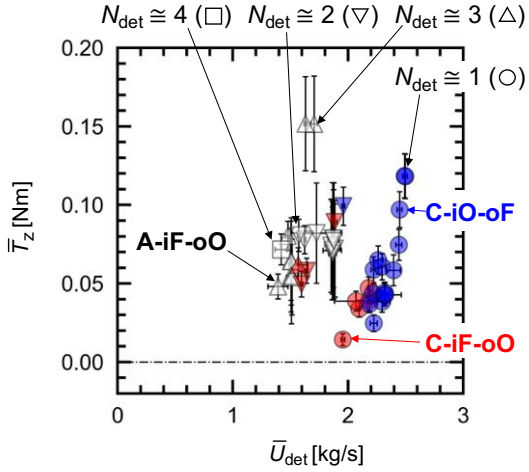

Figure 11: The torque vs the velocity of rotating detonation waves.

represents the deviation of light emission intensity. In this study, detonation waves in one direction were dominant enough during operation. In addition, the direction of T_z followed corresponded to the direction of detonation waves.

Figure 8 is the example time record of A-iF-oO. N_{det} changed 2 to 3 during the operation. Fig. 9 is the example time record of C-iF-oO. As the images of the detonation waves indicates, the light-emitting zone propagated along the outer wall. In the test, N_{det} changed 1 to 2. The change of T_z was larger in the example case of C-iF-oO than the one of A-iF-oO. In order to distinguish the difference, a single test was separated into multiple cases when N_{det} changed during the operation (S1 and S2 in Fig. 8-9). The time mean value during each section was defined as the representative value (with an over bar).

Fig. 10 is the comparison of T_z and $\dot{m}$. While cylindrical RDEs decrease the wetted perimeter length, it generated the same order of T_z as annular RDEs. Fig. 11 is the result of T_z and U_{det}. In most cases of

Cylindrical RDEs, U_{det} was larger than the cases of annular RDEs. Thus, larger τ_θ derived from the faster detonation waves generated the same order of T_z. Fig. 12 is the comparison of τ_θ calculated by assuming τ_θ on the contact surface of the wall and light-emitting zone generated T_z. In some cases of C-iO-oF, U_{det} was around 2.5 km/s. Due to the faster rotating detonation waves, these cases generated larger amount of τ_θ.

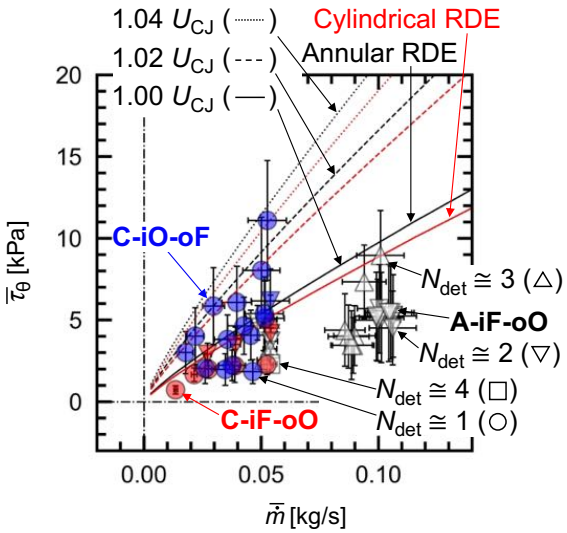

Figure 12: The azimuthal component of shear stress vs the mass flow rate.

4 Conclusion

While the wetted perimeter is smaller in the case of cylindrical RDEs than annular RDEs, cylindrical RDEs generated the same order of the torque around the thrust axis as annular RDEs. The propagation velocity of rotating detonation waves in Cylindrical RDEs was faster than in Annular RDEs in this study. Thus, because the faster rotating detonation waves generated the larger amount of the azimuthal component of the shear stress, the same order of torque generated in the case of cylindrical RDEs.

Acknowledgments

The rotating detonation engine development was subsidized by a “Study on Innovative Detonation Propulsion Mechanism,” Research- and-Development Grant Program (Engineering) from the Institute of Space and Astronautical Science, the Japan Aerospace Exploration Agency (JAXA). The fundamental device development was subsidized by a Grant-in-Aid for Specially Promoted Research No. 19H05464, a Grant-in-Aid for Scientific Researches (A) No. 24246137, and (B) No. 17H03480 from the Japan Society for the Promotion of Science. The six-axis force sensor was manufactured by Leptorino Company, Ltd.

References

[1] Wolanski, P., “Detonative Propulsion,” Proceedings of the Combustion Institute, Vol. 34, No. 1, 2013, pp. 125–158.

[2] Yokoo, R., Goto, K., Kim, J., Kawasaki, A., Matsuoka, K., Kasahara, J., Matsuo, A., and Funaki, I., “Propulsion Performance of Cylindrical Rotating Detonation Engine,” AIAA Journal, Vol. 58, No. 12, 2020, pp. 5107–5116.

[3] Sawada, S., Goto. K., Ishihara, K., Kawasaki, K., Matsuoka, K., Kasahara, J., Matsuo, A., Funaki, I., "Torque Around the Axial Direction on Rotating Detonation Engines," Journal of Propulsion and Power, Vol. 38, No. 1, 2022.

[4] Braun, J., Falempin, F, Paniagua, G., “Energy analysis of a detonation combustor with a bladeless turbine, a propulsion unit for subsonic to hypersonic flight,” Energy Conversion and Management Vol.262, 15 June 2022, 115491.

[5] Chacon, F., and Gamba, M., “Detonation Wave Dynamics in a Rotating Detonation Engine,” AIAA Scitech 2019 Forum, AIAA Paper 2019- 0198, 2019.